


Oscillations in the 45–5000 MHz Radio Spectrum of the 18 April 2014 Flare

Marian Karlický¹ · Ján Rybák²  · Christian Monstein³

© Springer

Abstract Using a new type of oscillation map, made from the radio spectra by the wavelet technique, we study the 18 April 2014 M7.3 flare (SOL2014-04-18T13:03:00L245C017). We find a quasi-periodic character of this flare with periods in the range 65–115 seconds. At the very beginning of this flare, in connection with the drifting pulsation structure (plasmoid ejection) we find the 65–115 s oscillation phase drifting slowly towards lower frequencies, which indicates an upward propagating wave initiated at the start of the magnetic reconnection. In the drifting pulsation structure many periods (1–200 seconds) are found documenting multi-scale and multi-periodic processes. On this drifting structure fiber bursts with a characteristic period of about one second are superimposed, whose frequency drift is similar to that of the drifting 65–115 s oscillation phase. We also check periods found in this flare by *EUV Imaging Spectrometer* (EIS)/*Hinode* and *Interface Region Imaging Spectrograph* (IRIS) observations. We recognize the type III bursts (electron beams) as proposed, but their time coincidence with the EIS and IRIS peaks is not very good. This is probably due to the radio spectrum being a whole-disk record consisting of all bursts from any location while the EIS and IRIS peaks are emitted only from locations of slits in the EIS and IRIS observations.

Keywords: Sun: flares — Sun: radio radiation — Sun: oscillations

✉ J. Rybák
rybak@astro.sk

¹ Astronomical Institute, Academy of Sciences of the Czech Republic, 251 65 Ondřejov, Czech Republic

² Astronomical Institute, Slovak Academy of Sciences, Tatranská Lomnica, Slovakia

³ Institute for Astronomy, ETH Zurich, CH-8093 Zurich, Switzerland

1. Introduction

In X-ray, ultraviolet and radio emissions of solar flares, oscillations and waves are commonly observed (Roberts, Edwin, and Benz, 1984; Fárník, Karlický, and Švestka, 2003; Wang *et al.*, 2005; Nakariakov *et al.*, 2006, 2010; Kumar, Nakariakov, and Cho, 2016).

These oscillations have periods ranging from sub-seconds to tens of minutes (Mészárosová *et al.*, 2006; Tan, 2008; Karlický, Zlobec, and Mészárosová, 2010; Kupriyanova *et al.*, 2010; Mészárosová, Rybák, and Karlický, 2011; Huang *et al.*, 2014; Nisticò, Pascoe, and Nakariakov, 2014).

For overviews of oscillations and waves, and their models, see the papers by Nakariakov and Melnikov (2009), Van Doorselaere, Kupriyanova, and Yuan (2016), and Nakariakov *et al.* (2016).

In several papers various types of oscillations and waves were already numerically studied: hot coronal loop oscillations (Ofman and Wang, 2002), slow MHD waves in solar coronal magnetic fields (De Moortel and Hood, 2003), acoustic oscillations in solar and stellar flaring loops (Nakariakov *et al.*, 2004), short quasi-periodic MHD waves in coronal structures (Nakariakov, Pascoe, and Arber, 2005), slow magnetosonic standing waves in a solar coronal loop (Selwa, Murawski, and Solanki, 2005), impulsively generated slow acoustic waves in a solar coronal loop (Jelínek and Karlický, 2009), impulsively generated wave trains in coronal loops (Jelínek and Karlický, 2010), slow magnetoacoustic standing modes in a gravitationally stratified solar coronal arcade (Konkol *et al.*, 2010), slow magnetosonic waves in active region loops (Ofman, Wang, and Davila, 2012), standing kink modes in coronal loops (Pascoe and De Moortel, 2014), and magnetoacoustic waves propagating along a dense slab and Harris current sheet (Mészárosová *et al.*, 2014).

Recently, searching for signatures of the fast magnetosonic waves in the 1 August 2010 event, we developed a new type of map of oscillations based on the wavelet transform analysis of radio spectra (Karlický and Rybák, 2017).

In the present paper, we construct such maps of oscillations for the 18 April 2014 flare that looks to be rich in various oscillations. Namely, oscillations were recognized in the global X-ray flux detected by the *Fermi/Gamma-ray Burst Monitor* (GBM) instrument as well as in the spatially localized UV measurements of the *Interface Region Imaging Spectrograph* (IRIS) and *EUV Imaging Spectrometer* (EIS)/*Hinode* instruments (Brosius and Daw, 2015, Brosius, Daw, and Inglis, 2016 and Brannon, Longcope, and Qiu, 2015). Moreover as shown by Brosius, Daw, and Inglis (2016) in the interval of these oscillations the profiles of the O IV – Fe XVI lines were redshifted and the electron densities in the regions of the Fe XIV and Mg VII line generation were $4.6 \times 10^{10} \text{ cm}^3$ and $7.8 \times 10^9 \text{ cm}^3$, respectively. Further quasi-periodic oscillations in both position and Doppler velocities were found in small-scale substructure within the flare ribbon (Brannon, Longcope, and Qiu, 2015).

Therefore, in the paper, we not only want to know what oscillations are present in radio emission of this flare, but we want to compare them with the oscillations detected in X-rays and in the IRIS and EIS UV observations. Of

course, we also want to confirm or reject the beam origin idea of EIS oscillation proposed by Brosius, Daw, and Inglis (2016).

Because we analyze the radio spectra in decimetric and metric ranges, where most of bursts are generated by the plasma emission mechanism (the emission frequency depends on the plasma density in the radio source), the frequency of oscillations on the map gives us an information about the altitude of these oscillations in the solar atmosphere. Furthermore, a possible frequency drift of oscillation phases indicates propagating waves.

The paper is structured as follows: In Section 2 we present the data and methods of analysis. The results and their interpretations are summarized in Section 3. Conclusions are in Section 4.

2. Data and Methods of Their Analysis

The radio spectrum was acquired during the 18 April 2014 flare (*Hinode* Flare Catalog - event number 103690 (Watanabe, Masuda, and Segawa, 2012)). This flare, classified as a GOES M7.3 flare, started at 12:31 UT, peaked at 13:03 UT, and ended at 13:20 UT in NOAA active region 12036 (S17W40). For more details about radio observations of this flare, see the recent paper by Carley, Vilmer, and Gallagher (2016).

The overall radio spectrum selected for our analysis consists of two e-Callisto (International Network of Solar Radio Spectrometers) radiospectrographs, and two Ondřejov radiospectrographs for the time interval 12:40–13:10 UT. The details of the observations are as follows:

- The *Bleien BLEN7M radiospectrograph* is located at Bleien, Switzerland. Its frequency range, mean frequency resolution, and temporal resolution are 175–870 MHz, 3.61 MHz, and 0.25 second respectively.
- The *Glasgow Small Radio Telescope* is located at Acre Road Observatory, Glasgow, Scotland. Its frequency range, mean frequency resolution, and temporal resolution are 81–45 MHz, 0.2 MHz, and 0.25 second, respectively.
- The *Ondřejov radiospectrograph RT5* is located at Ondřejov, Czech Republic. Radiospectrograph frequency range, frequency resolution, and temporal resolution are 800–2000 MHz, 4.7 MHz, and 10 ms, respectively (Jiříčka and Karlický, 2008).
- The *Ondřejov radiospectrograph RT4* is located at Ondřejov, Czech Republic. Radiospectrograph frequency range, frequency resolution, and temporal resolution are 2000–5000 MHz, 11.6 MHz, and 1 second, respectively (Jiříčka *et al.*, 1993).

During data selection all records available in the e-Callisto archive¹ for this particular time interval are checked. Only radiospectrograms of the best quality in the frequency ranges of interest are selected. Those data are adapted using the dedicated software from the ethz library in SolarSoft (Freeland and Handy,

¹see http://soleil180.cs.technik.fhnw.ch/solarradio/data/2002-20yy_Callisto/ .

1998) according the dedicated manual². The e-Callisto data are not calibrated in intensity and these data are a logarithmic representation of solar radio burst activity (Benz, Monstein, and Meyer, 2005).

All radio data are re-sampled to the final temporal sampling of 1 second except a particular additional data set of the Ondřejov 800–2000 MHz data in the time interval 12:47–12:49 UT, for which the 0.1 second sampling is used.

At some frequencies, artificial radio noise heavily affects the acquired signal. Such parts of the data are excluded and they are marked by black bands in all plots of the radiospectrograms. The general radio spectrum composed from the individual radio spectra of all four radiospectrographs is shown in the left column of Figure 3.

For analysis of the radio spectra we utilize a novel method introduced in our recent article (Karlický and Rybák, 2017). The wavelet transform (WT) is a core of this method providing a clear detection of time–frequency evolution of the significantly strong radio signal wave–patterns. This method detects the identified wave–pattern signal power which is located in the selected period range at any temporal moment and radio frequency.

Due to possible multiplicity of the non–stationary periodicities the investigated periodicities are limited to maximum power in a selected narrower WT period range of particular interest. The WT computational algorithm of Torrence and Compo (1998) is applied to individual radio–signal time series. The Morlet mother wavelet, consisting of a complex sine wave modulated by a Gaussian, is selected to search for radio signal variability, with the non–dimensional frequency ω_0 satisfying the admissibility condition (Farge, 1992). The WT is calculated for the period range from 10 to 600 seconds (or from 1 to 200 seconds) with scales sampled as fractional powers of two with $\delta j = 0.4$, which is small enough to give an adequate sampling in scale, a minimum scale $s_j = 9.64$ seconds (0.96 second) and a number of scales $N = 101$. Both the calculated significance of the derived WT periodicities and the cone–of–influence are taken into account as described in Karlický and Rybák (2017). The value of the confidence level is set to 99 % for this article.

As a reference for the X–ray emission of the flare we select the *Fermi* mission *Gamma-ray Burst Monitor* (*Fermi*/GBM, Meegan *et al.*, 2009) data in the 26–50 keV range. Dedicated *Object Spectral Executive* (OSPEX) software from the *spex* library of SolarSoft (Freeland and Handy, 1998) is exploited for data preparation. The same data set has been analyzed also in the article by Brosius, Daw, and Inglis (2016), where more instrumental details can be found.

3. Results

A global overview of the 18 April 2014 solar flare is shown in Figure 1 using the *Fermi*/GBM 26–50 keV light curve and the particular radio fluxes at 5000,

²see http://www.e-callisto.org/Software/phoenix_howto.html.

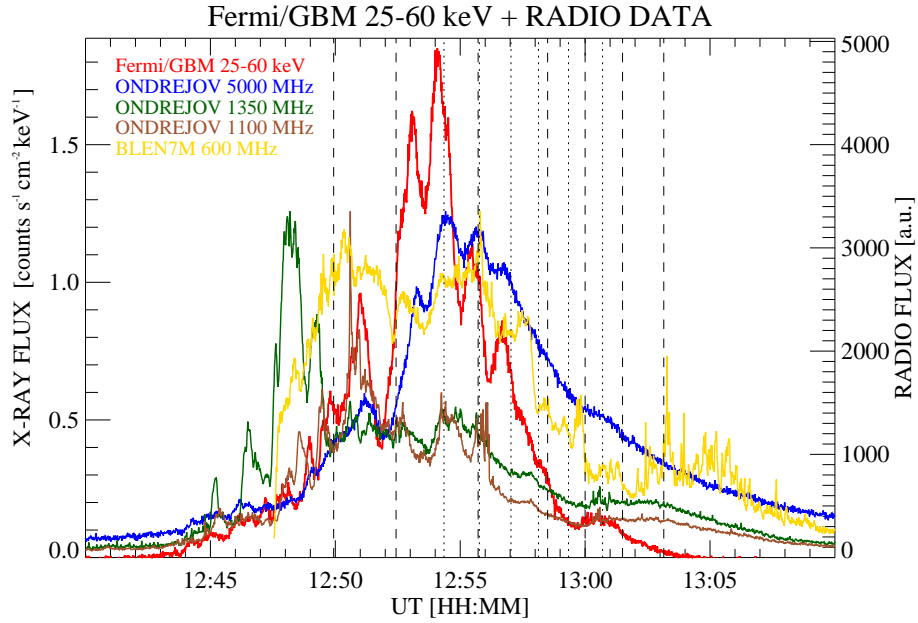


Figure 1. Global overview of the 18 April 2014 solar flare: *Fermi*/GBM 26–50 keV light curve and the radio fluxes at 5000, 1350, 1100, and 600 MHz. The vertical dotted lines designate times of the EIS emission peaks and the vertical dashed lines show times of the IRIS emission peaks (for exact time and spatial location information on these peaks see Section 3).

1350, 1100, and 600 MHz. All these full-disk flux curves reveal a quasi-periodic behavior with peaks which are more or less synchronized in general.

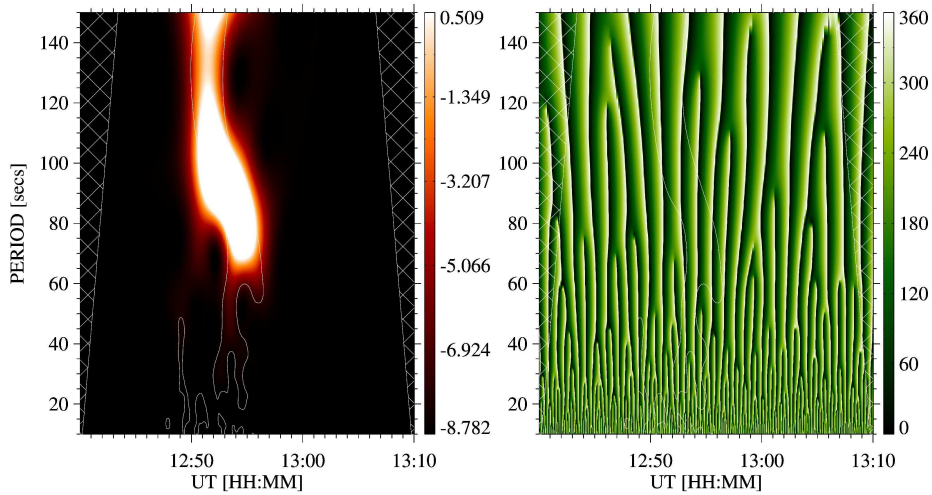


Figure 2. Wavelet power and phase spectra of the *Fermi*/GBM 26–50 keV X-ray emission. The white contours mark the time–frequency domain area of the statistically significant periodicities while the cross-hatched areas show the cone-of-influence.

In Figure 1 the vertical dotted lines designate times of EIS emission peaks (12:54:21, 12:55:46, 12:57:02, 12:58:08, 12:59:20, and 13:00:42 UT) (Brosius, Daw, and Inglis, 2016), and the vertical dashed lines show times of IRIS emission peaks (12:49:56, 12:52:26, 12:55:43, 12:58:30, 13:00:00, 13:01:30, and 13:03:09 UT) (Brosius and Daw, 2015). However, these emission peaks are detected in the spatially very localized positions of the slits of these instruments (EIS: $X = 512 \pm 1''$, $Y = -219 \pm 2''$, IRIS: $X = 551 \pm 0.16''$, $Y = -186.4 \pm 0.16''$).

It is clearly seen that some of these EIS and IRIS peaks coincide well with the presented hard X-ray and radio fluxes peaks, for example, at 12:54:21 or 12:55:46 UT. On the other hand, in the time interval 12:57–13:00 UT, where several EIS and IRIS peaks are observed, the hard X-ray 26–50 keV flux and the 5000, 1350, and 1100 MHz radio flux plots are more or less smooth, except for the peaks present in the 600 MHz radio flux plot.

To know the characteristic periods in these processes, we analyze the hard X-ray *Fermi*/GBM 26–50 keV emission of this flare. The resulting wavelet power and phase spectra are shown in Figure 2. As seen here, the flare in hard X-rays has in the time interval 12:49–12:57 UT a characteristic period at about 115 seconds which displays shortening in the course of this time interval down to about 65 seconds. This result, derived using the WT method, is in coincidence with the previously derived value of 72 ± 2.7 seconds (Brosius, Daw, and Inglis, 2016) which was determined just from temporal moments of the peaks in the interval 12:53–12:57 UT. Our initial value of 115 seconds reflects the appearance of the hard X-ray peak located at 12:51 UT which appears before the very regular next four peaks.

Knowing the interval of characteristic periods in hard X-rays, we construct the oscillations map for these periods for all radio spectra in the 45–5000 MHz frequency range. The radio spectra (Figure 3, left column) as well as the corresponding maps of phase (pink bands overplotted on the radio spectra) are presented in Figure 3 (right column). Note that lower frequencies in this figure are presented above higher ones, which expresses that the emission at lower frequencies is generated at higher heights in the solar atmosphere than that at higher frequencies. Thus, the radio spectra and phase maps give us information about flare processes and oscillations in the vertical direction in the solar atmosphere.

As seen in the radio spectra, in a broad range of frequencies from 45 to 5000 MHz (Figure 3, left column), the flare appears in radio at about 12:44 UT with a so-called drifting pulsation structure (DPS), lasting till 12:53 UT in the 800–1600 MHz range and also appears as a series of type III bursts in the 45–80 MHz range. At higher frequencies (2000–5000 MHz) there is a continuum that starts at about the same time as the DPS and has its maximum at 12:54 UT in coincidence with the hard X-ray maximum. In the 175–862 MHz range we see broadband emission (12:47–13:08 UT) consisting of fast-drifting type III bursts and two slowly drifting bursts (at 12:49–12:55 UT and 12:54–12:56 UT in the 500–250 MHz range), designated by Carley, Vilmer, and Gallagher (2016) as Continuum A and Continuum B, which look to be the high-frequency precursors of the type II burst observed at 12:55–13:07 UT in the 45–80 MHz range.

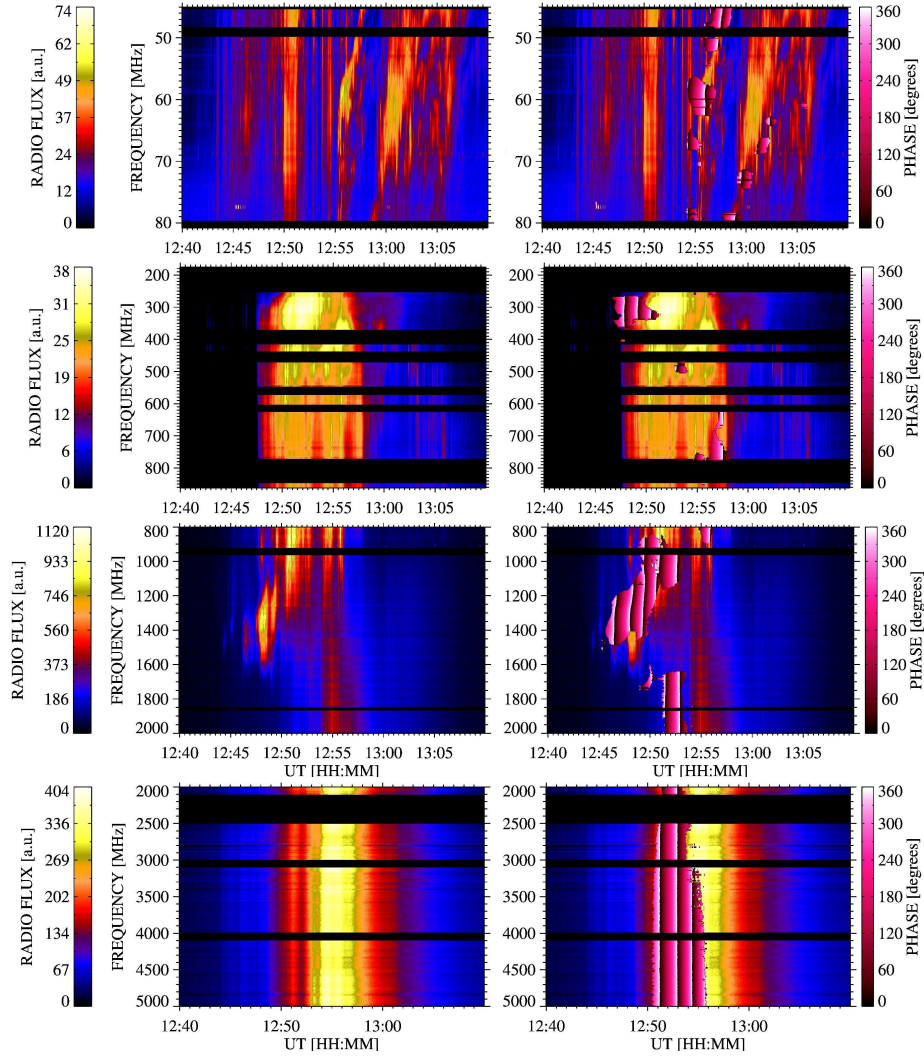


Figure 3. Left column: the radio spectra observed by the e-Callisto radio spectrometers (Glasgow: 45–80 MHz, BLEN7M: 175–862 MHz), and by the Ondřejov radiospectrographs (800–2000, and 2000–5000 MHz). Right column: the same radio spectra and the corresponding phase maps overplotted on these radio spectra for periods detected within the 65–115 second range. The black lines in the phase pink bands correspond to zero phases.

In the right column of Figure 3, there are the corresponding maps of oscillations with periods in the selected 65–115 seconds interval. These oscillations are mostly at higher frequencies starting at about 12:45 UT at 1400 MHz. In the 250–5000 MHz range they are nearly synchronized (within a few seconds). Only at the beginning of the radio flare in the interval 12:45–12:49 UT and 1200–1500 MHz range we see some drift of the oscillation phase. Namely, the phase drift in the bursts generated by the plasma emission mechanism indicates a propagating wave with a period 65–115 seconds. Details about these phase drifts

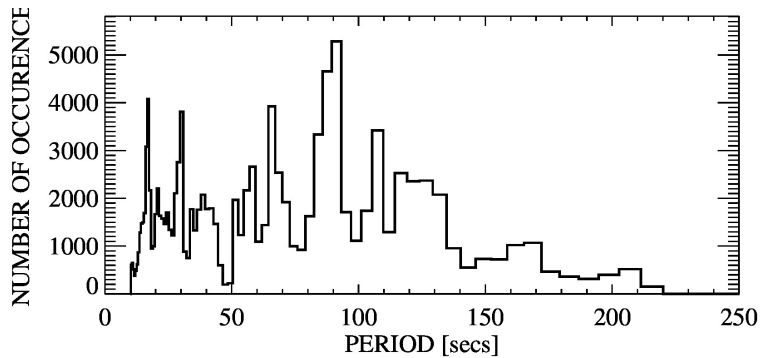


Figure 4. The histogram of the periods in the 800–2000 MHz radio spectrum for the 12:44–12:54 UT time interval.

are given below. At lower frequencies, in the 45–80 MHz range, the oscillations with a 65–115 seconds period as a part of a type II burst are detected later than those at higher frequencies and sporadically only.

3.1. Phase Maps of the Drifting Pulsation Structure Observed in the 800–2000 MHz Range

As mentioned above the flare radio emission starts in the DPS observation at 12:43 UT and around 1400 MHz. This relatively narrowband (≈ 400 MHz) emission consists of many fast drifting pulses, and drifts as a whole from 1400 MHz to 800 MHz (Figure 3, left column, third panel and detailed view in Figure 5, top panel). Models of such emission were presented by Kliem, Karlický, and Benz, 2000, Karlický, 2004, Karlický and Bárta, 2007, Bárta, Vršnak, and Karlický, 2008, Karlický, Bárta, and Rybák, 2010, Bárta *et al.*, 2011, Karlický and Bárta, 2011, and Nishizuka *et al.*, 2015. It was proposed that the DPS is the signature of a plasmoid formed in the early phase of the fast magnetic reconnection in the flare current sheet. During the plasmoid formation electrons are rapidly accelerated (Karlický, 2008). A part of these super-thermal electrons are trapped in the plasmoid, where they generate the plasma waves which are then transformed into electromagnetic (radio) waves observed as the DPS. If the injection of super-thermal electrons into the plasmoid is quasi-periodic then DPS is formed from separate pulses like the DPS presented by Kliem, Karlický, and Benz (2000). On the other hand, if the injection is more or less continuous then DPS looks like a narrowband drifting continuum with some pulses (present case). Owing to the limited range of densities inside the plasmoid, the emission frequencies are limited as well. Therefore the frequency range of the DPS gives us information about the density range in the plasmoid. Using the relation for the plasma density $n_e(\text{cm}^{-3}) = f^2/8.1 \times 10^{-5}$, where f is the observed frequency in MHz (Kundu, 1965), we obtain $n_e = 1.8 \times 10^{10} - 3.2 \times 10^{10} \text{ cm}^{-3}$ at 12:48 UT.

The DPS slowly drifts to lower frequencies with a frequency drift -1.66 MHz s^{-1} . To estimate the velocity of the corresponding plasmoid some model of the solar atmosphere has to be used. There are several such models as presented

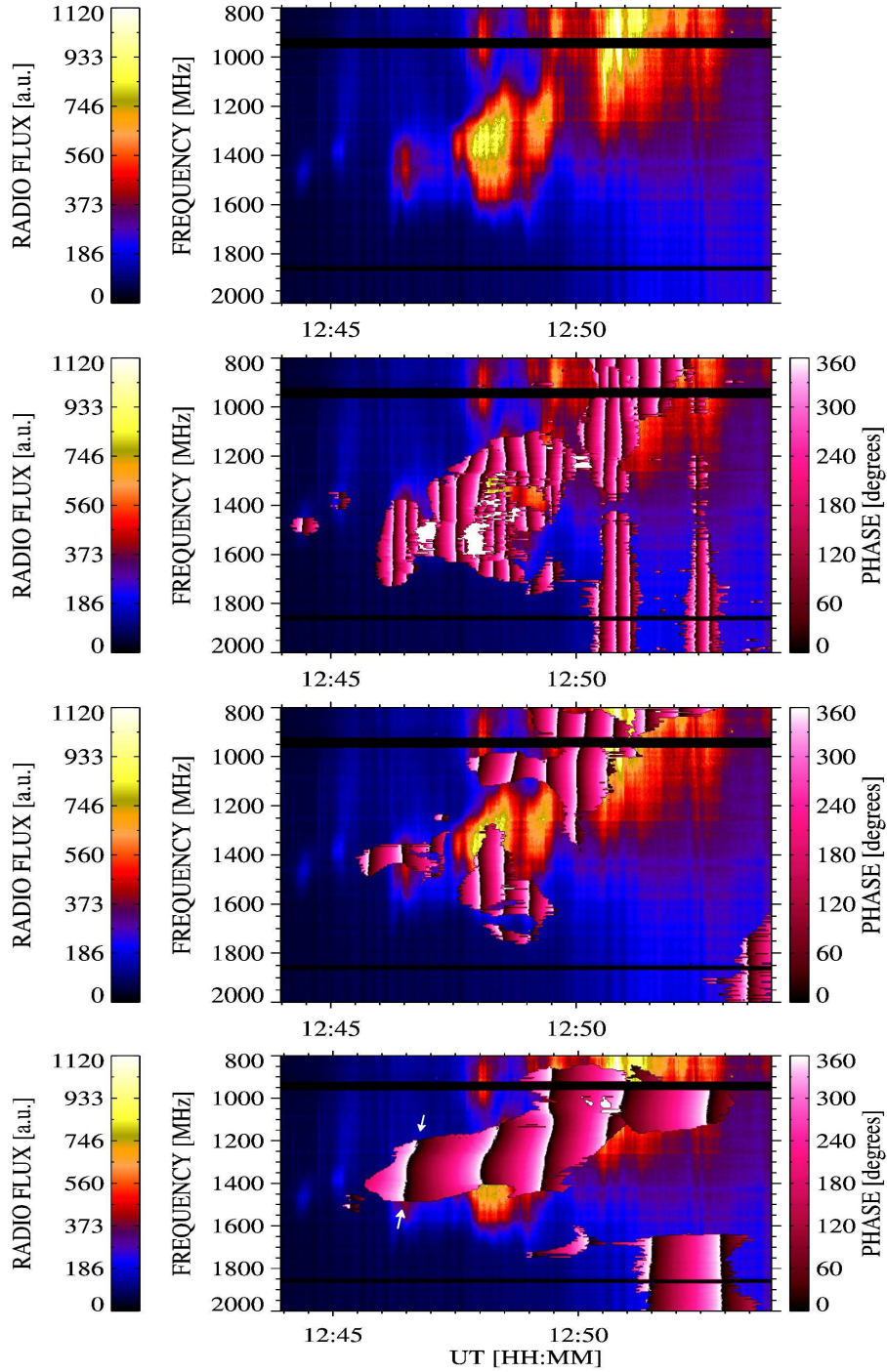


Figure 5. The 800–2000 MHz Ondřejov radio spectrum in the 12:44–12:54 UT time interval (top panel) and the wavelet phase maps overplotted on this radio spectrum for period ranges 10–30, 30–50, and 65–115 seconds (bottom panels). The white arrows in the bottom panel show the zero phase drifting from high to lower frequencies.

in the papers by Pohjolainen *et al.* (2007); Kumar and Cho (2013); Carley, Vilmer, and Gallagher (2016). However, for the frequencies of the present DPS (above 800 MHz and the fundamental emission of DPS), only the Aschwanden model (Aschwanden, 2002) can be used. Therefore, in the following we use the Aschwanden model and its multiplied version. We start with the Aschwanden model, but consider also that the density in the plasmoid is higher than outside of the plasmoid. It can be shown that in the case of the plasmoid observed in the 5 October 1992 flare (Ohyama and Shibata, 1998), the density inside the plasmoid was 6.9 times higher than outside. If we assume for the present DPS (plasmoid) the same density contrast as in the 5 October 1992 plasmoid, the derived upward velocity of the plasmoid is 28 km s^{-1} . Now, let us utilize the result of Carley, Vilmer, and Gallagher (2016). Namely, they determined the level of the second harmonic frequency 445 MHz ($n_e = 6.11 \times 10^8 \text{ cm}^{-3}$) in this flare to be at the height 140 Mm. Multiplying the Aschwanden model by the factor 10.5, we obtain the same density at the same height. Then using this multiplied Aschwanden model and the same procedure mentioned above, we determine the upward velocity of the plasmoid to be 73 km s^{-1} . (Note that according to the DPS model (Bárta, Vršnak, and Karlický, 2008) the velocity of the plasmoid is given by the tension of surrounding magnetic field lines. Thus, the plasmoid velocity can be in the interval from zero velocity (motionless case) up to the local Alfvén velocity (maximum velocity case). The estimated plasmoid velocities are realistic because they are lower than the Alfvén velocity expected in the magnetic reconnection site.) The negative frequency drift of the DPS shows that the plasmoid moves upward in the solar atmosphere. Namely, during its upward motion the density as well as plasma frequency inside the plasmoid decreases and thus the DPS drifts towards lower frequencies. The fast-drifting pulses show individual injection of the super-thermal electrons into the plasmoid. Note that other super-thermal electrons that are not trapped in the plasmoid escape in the upward direction as the observed type III bursts and downwards generating the observed continuum.

The DPSs are very important bursts in any solar flare and therefore we make a detailed analysis of the periodicities in a shorter time interval of 12:44–12:54 UT where DPS appears (Figure 5, top panel). We compute the histogram of the significant periods in this radio spectrum (Figure 4). As seen here, the radio spectrum consists of periods in a broad range from seconds up to 200 seconds, which agrees with the idea of cascading (multi-scale and multi-periodic) processes in the flare magnetic reconnection (Karlický and Bárta, 2011 and Bárta *et al.*, 2011).

The oscillation maps for this radiospectrogram for several intervals of periods are shown in Figure 5 together with the radiospectrogram (top panel). They confirm that the processes generating the DPS are multi-scale and multi-periodic as the significant oscillations are of a co-temporal and co-spatial appearance. An interesting aspect is that the zero phase (black line) with the period interval 65–115 seconds drifts from a frequency of about 1500 MHz to 1200 MHz in the time interval from 12:46:30–12:46:40 UT (Figure 5, bottom part, see the white arrows). The frequency drift is about -30 MHz s^{-1} , which corresponds to velocities of about 500 km s^{-1} and 1300 km s^{-1} in the Aschwanden and the 10.5

× Aschwanden density models, respectively, where we use also the correction to the enhanced density in the plasmoid. We propose that this drift indicates the presence of a fast magnetoacoustic wave propagating upwards in the solar atmosphere. Note that such a wave was detected in the numerical simulations just after a sudden enhancement of the resistivity at the start of the magnetic reconnection in the current sheet Karlický (1988). We think that this wave modulates the plasma density in the radio source and thus modulates the radio emission as proposed in the papers by Karlický, Mészárosová, and Jelínek (2013) and Karlický (2013).

Remarkable features detected in the 800–2000 MHz frequency range only during the temporal interval of just 120 seconds (12:47–12:49 UT) stimulate us to analyze this radio spectrum using 0.1 second data temporal sampling (Figure 6). Here, the periods 1.1–1.7 and 1.8–3.0 seconds are recognized not only in the DPS structure, but also in the type III bursts in the 800–1100 MHz range at 12:48:00–12:48:20 UT. The phases overplotted on DPS, which start at about 1400 MHz and at 12:48:07 UT (and last till 12:48:11 UT) drift towards lower frequencies with a frequency drift of about -28 MHz s^{-1} . Moreover, if we enlarge the phase map in the 1100–1300 MHz range at 12:48:21–12:48:32 UT, we can see phases drifting negatively as well as positively. A detailed analysis of the original radio spectrum (Figure 6, top panel) reveals that these drifting phases correspond to very weak fiber bursts superimposed on the DPS structure. Their frequency drift is of course the same as that of their phases (-28 MHz s^{-1}) because they occur on the radio spectrum repeatedly with a characteristic period of about second.

Generally, there are three types of models of the fiber bursts. Models interpreting their frequency drift based on whistler waves (Mann, Karlický, and Motschmann, 1987), models interpreting this drift with Alfvén waves (Treumann, Guedel, and Benz, 1990), and models considering the fast magnetoacoustic waves (Kuznetsov, 2006; Karlický, Mészárosová, and Jelínek, 2013). The frequency drift of the 65–115 s oscillation phase found at the beginning of DPS at 12:46:30–12:46:40 UT (Figure 5, bottom part) (-30 MHz s^{-1}) is comparable to that of the fiber bursts superimposed on DPS (Figure 6) (-28 MHz s^{-1}). Therefore, if both these features are generated in the same region with similar plasma parameters and the drifting phase at 12:46:30–12:46:40 UT is a signature of the fast magnetoacoustic wave then the fiber bursts in the present case are in better agreement with the fast magnetoacoustic-wave (period about 1 second) type or Alfvén-wave type models of fibers than that based on the whistler waves. For details, see the papers by Mann, Karlický, and Motschmann (1987); Treumann, Guedel, and Benz (1990); Karlický, Mészárosová, and Jelínek (2013).

3.2. The Phase Maps of the 175–862 MHz Radio Spectrum in the Time Interval of EIS Oscillations

Brosius, Daw, and Inglis (2016) presented quasi-periodic ($P \approx 75.6 \pm 9.2 \text{ s}$) intensity fluctuations in emission lines of O IV, Mg VI, Mg VII, Si VII, Fe XIV, and Fe XVI during the flare soft X-rays rise in the 12:54–13:01 UT time interval (see also Figure 1 in the present paper for the hard X-ray flux plot). They

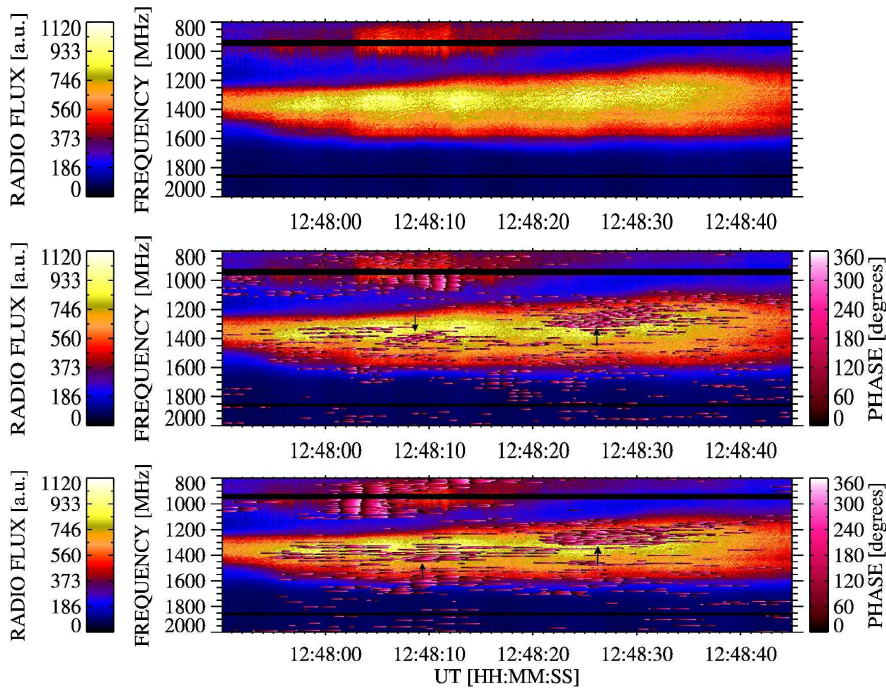


Figure 6. The 800–2000 MHz Ondřejov radio spectrum in the 12:47:50–12:48:45 UT time interval (top panel) and the wavelet phase maps overplotted on this radio spectrum for period ranges 1.1–1.7 and 1.8–3.0 seconds (middle and bottom panels, respectively). The black arrows in the middle and bottom panels show the regions with drifting phases.

proposed that these fluctuations are by a series of energy injections into the chromosphere by non-thermal electron beams. Because in that paper there is no direct evidence of these beams (the hard X-ray emission in this time interval is smooth, see Figure 1), we look for signatures of these beams in the radio range. Seeing the plots of radio fluxes on several selected frequencies, we find that only the 600 MHz record shows some distinct variations during the time interval of our interest. Therefore, we focus our attention on the radio spectrum in the 175–862 MHz range (Figure 7, top part). In this radio spectrum (at 12:55–13:00 UT in the 450–862 MHz range) we see groups of fast-drifting type III bursts. These bursts are considered to be signatures of electron beams which thus supports the explanation of emission line fluctuations proposed by Brosius, Daw, and Inglis (2016).

To visualize the radio bursts even better, we form the new spectrum with long periods (above 200 s) removed. It is presented in Figure 7 (second part from the top) and the corresponding 600 MHz radio emission plot is the bottom panel of this figure. However, as expressed by the vertical lines in this 600 MHz plot an association between the type III burst and the EIS and IRIS peaks in some cases is good (*e.g.* at 12:55:46) and in other cases problematic. This is probably due to radio spectrum being a whole-disk record consisting of all bursts from any location, whereas the EIS and IRIS peaks come only from the particular spatial locations of the slits of the EIS and IRIS instruments.

We also check for a quasi-periodic character of the type III bursts in the studied 12:54–13:54 UT time interval. As shown in Figure 7 (third panel from the top) only in limited intervals of time and frequencies (12:55:40–12:57:30 UT, 550–800 MHz) do we find the 65–115 seconds period oscillations, which is the same period found in the *Fermi*/GBM 26–50 keV light curve.

In the time interval from 12:49 to 12:56 UT two slowly drifting features are observed in the 250–500 MHz range (Continuum A and Continuum B according to Carley, Vilmer, and Gallagher (2016)). As shown by Carley, Vilmer, and Gallagher (2016) the Continuum A source was stationary and the source of Continuum B moved with the velocity 397 km s^{-1} .

4. Conclusions

We find that the 18 April 2014 M7.3 flare event as a whole has a quasi-periodic character in the 65–115 seconds period interval. This quasi-periodic behavior is recognized not only in the *Fermi*/GBM hard X-ray emission, but also in radio waves over a broad range of frequencies. In most cases, similar to the 1 August 2010 C3.2 flare event (Karlický and Rybák, 2017), the phases of these 65–115 seconds oscillations are nearly synchronized (within a few seconds) over a very broad range of frequencies. Therefore, similar to the paper by Karlický and Rybák (2017), we explain this synchronization by fast electron beams (type III bursts) propagating through the solar corona, with acceleration modulated by a wave or an oscillation process with a period in the 65–115 seconds interval.

However, at the very beginning of the flare at the time of the plasmoid formation (expressed in radio as the DPS), in the phase map with the 65–115 seconds period, we find a negative drift of the phase which shows a propagating wave. We propose that this wave is the fast magnetoacoustic wave propagating from the plasmoid site upwards. Such a wave can be generated as follows: in the current sheet magnetic reconnection starts when the current sheet is sufficiently narrow, *i.e.* when the electric current density inside the current sheet is sufficiently high. If this current density overcomes some threshold then the anomalous resistivity can be suddenly generated (Norman and Smith, 1978). Such a sudden enhancement of the localized resistivity leads to a strong local heating and increase of the pressure, which generates magnetoacoustic waves. Such a wave was detected in the numerical simulations just after a sudden enhancement of the resistivity at the start of magnetic reconnection in the current sheet (Karlický, 1988). In fragmented reconnection (Bárta *et al.*, 2011; Karlický and Bárta, 2011) there can be several such regions with highly varying resistivity. They are located in space between plasmoids. The generated magnetoacoustic wave then propagates over or out of the plasmoids.

We think that this magnetoacoustic wave modulates the plasma density in the radio source and thus modulates the radio emission as proposed in the papers by Karlický, Mészárosová, and Jelínek (2013) and Karlický (2013), and produces the observed WT phase drift.

It is interesting that the frequency drift of this drifting phase (-30 MHz s^{-1}) (probably the fast magnetoacoustic wave) is comparable to that of fiber bursts

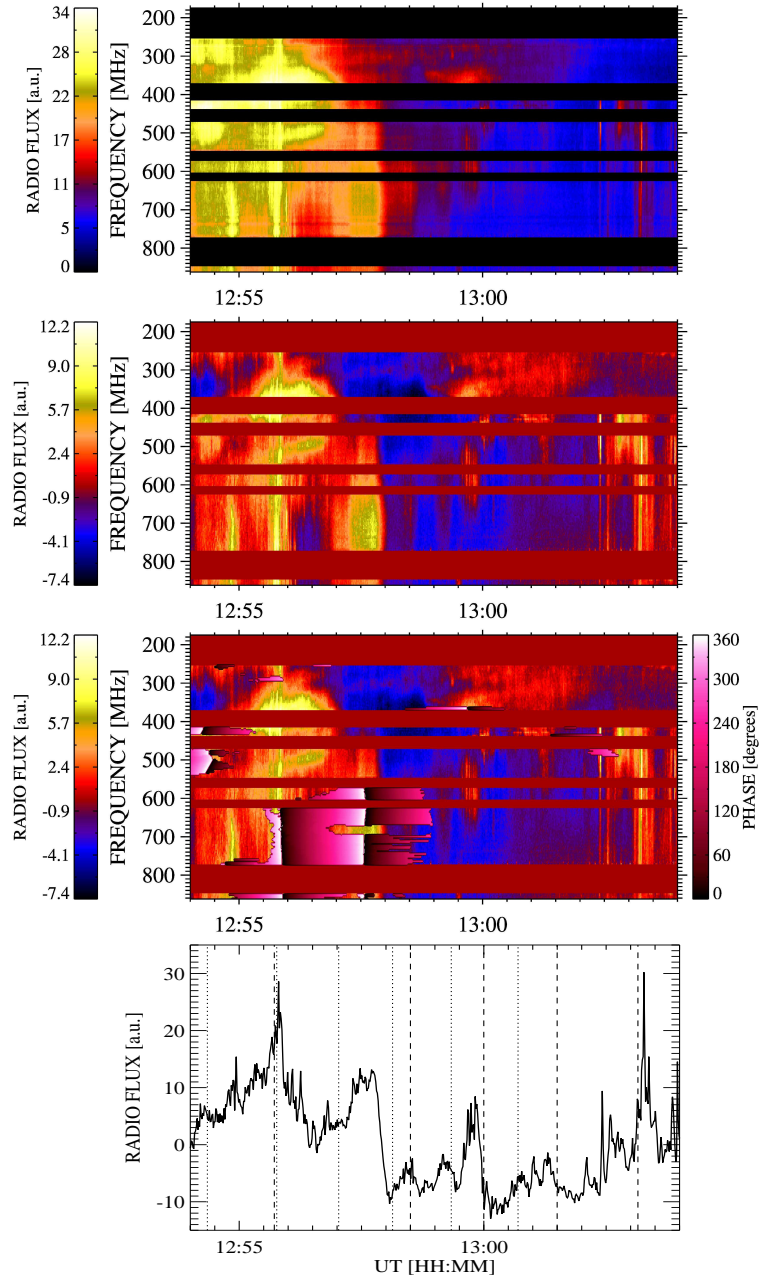


Figure 7. The 175–860 MHz Callisto Bleien radio spectrum in the 12:54–13:04 UT time interval: top – original spectrum; upper middle – adapted spectrum (long-term trend removed); bottom middle – adapted spectrum overplotted by the phase map for the period 65–115 s; bottom – an example of the adapted radio flux at the 600 MHz frequency. The vertical dotted and dashed lines in the 600 MHz plot designate times of the EIS and IRIS emission peaks, respectively (the same as in Figure 1).

superimposed on DPS (-28 MHz s^{-1}). In the present case, it could speak in favour of the fast magnetoacoustic-wave type or Alfvén-wave type models of fibers in comparison with the whistler-wave type model.

The drifting pulsation structure DPS reveals many periods ranging from 1 to 200 s. It indicates that the DPS is connected with a multi-scale and multi-periodic process. We even find fibers periodically repeated with a ≈ 1 second period and superimposed on the DPS.

We also check for the periods found in the EIS and IRIS spatially localized observations by Brosius, Daw, and Inglis (2016). In the 450–862 MHz range we recognize the type III bursts (electron beams) as proposed by Brosius, Daw, and Inglis (2016), but their time coincidence with the EIS and IRIS peaks is in some cases good and in others not so good. We think that this is due to the radio spectrum being a whole-disk record consisting of all bursts at any location. On the other hand, the EIS and IRIS peaks are emitted only from the locations of the slits in the EIS and IRIS observations, and the flare process evolves in time as well as in space.

Acknowledgments This research was supported by Grants 16–13277S and 17–16447S of the Grant Agency of the Czech Republic. This work was supported by the Science Grant Agency project VEGA 2/0004/16 (Slovakia). Help of the Bilateral Mobility Project SAV–16–03 of the SAS and CAS is acknowledged. This article was created by the realisation of the project ITMS No. 26220120029, based on the supporting operational Research and development program financed from the European Regional Development Fund. The authors are indebted to the Institute for Astronomy, ETH Zurich, and FHNW Windisch (Switzerland) and to the School of Physics and Astronomy of the University of Glasgow (Scotland, UK) for the Callisto data. This research has made use of NASA’s Astrophysics Data System. The wavelet analysis was performed with software based on tools provided by C. Torrence and G. P. Compo at <http://paos.colorado.edu/research/wavelets>.

Disclosure of Potential Conflicts of Interest

The authors declare that they have no conflicts of interest.

References

- Aschwanden, M.J.: 2002, Particle acceleration and kinematics in solar flares - A Synthesis of Recent Observations and Theoretical Concepts (Invited Review). *Space Sci. Rev.* **101**, 1. DOI. ADS.
- Bárta, M., Vršnak, B., Karlický, M.: 2008, Dynamics of plasmoids formed by the current sheet tearing. *Astron. Astrophys.* **477**, 649. DOI. ADS.
- Bárta, M., Büchner, J., Karlický, M., Skála, J.: 2011, Spontaneous Current-layer Fragmentation and Cascading Reconnection in Solar Flares. I. Model and Analysis. *Astrophys. J.* **737**, 24. DOI. ADS.
- Benz, A.O., Monstein, C., Meyer, H.: 2005, Callisto A New Concept for Solar Radio Spectrometers. *Solar Phys.* **226**, 143. DOI. ADS.
- Brannon, S.R., Longcope, D.W., Qiu, J.: 2015, Spectroscopic Observations of an Evolving Flare Ribbon Substructure Suggesting Origin in Current Sheet Waves. *Astrophys. J.* **810**, 4. DOI. ADS.

- Brosius, J.W., Daw, A.N.: 2015, Quasi-periodic Fluctuations and Chromospheric Evaporation in a Solar Flare Ribbon Observed by IRIS. *Astrophys. J.* **810**, 45. DOI. ADS.
- Brosius, J.W., Daw, A.N., Inglis, A.R.: 2016, Quasi-periodic Fluctuations and Chromospheric Evaporation in a Solar Flare Ribbon Observed by Hinode/EIS, IRIS, and RHESSI. *Astrophys. J.* **830**, 101. DOI. ADS.
- Carley, E.P., Vilmer, N., Gallagher, P.T.: 2016, Radio Diagnostics of Electron Acceleration Sites During the Eruption of a Flux Rope in the Solar Corona. *Astrophys. J.* **833**, 87. DOI. ADS.
- De Moortel, I., Hood, A.W.: 2003, The damping of slow MHD waves in solar coronal magnetic fields. *Astron. Astrophys.* **408**, 755. DOI. ADS.
- Farge, M.: 1992, Wavelet transforms and their applications to turbulence. *Annual Review of Fluid Mechanics* **24**, 395. DOI. ADS.
- Fárník, F., Karlický, M., Švestka, Z.: 2003, Hard x-ray Pulsations in the Initial Phase of Flares. *Solar Phys.* **218**, 183. DOI. ADS.
- Freeland, S.L., Handy, B.N.: 1998, Data Analysis with the SolarSoft System. *Solar Phys.* **182**, 497. DOI. ADS.
- Huang, J., Tan, B., Zhang, Y., Karlický, M., Mészárosóvá, H.: 2014, Quasi-Periodic Pulsations with Varying Period in Multi-Wavelength Observations of an X-class Flare. *Astrophys. J.* **791**, 44. DOI. ADS.
- Jelínek, P., Karlický, M.: 2009, Computational study of impulsively generated standing slow acoustic waves in a solar coronal loop. *European Physical Journal D* **54**, 305. DOI. ADS.
- Jelínek, P., Karlický, M.: 2010, Impulsively Generated Wave Trains in a Solar Coronal Loop. *IEEE Transactions on Plasma Science* **38**, 2243. DOI. ADS.
- Jiříčka, K., Karlický, M.: 2008, Narrowband Pulsating Decimeter Structure Observed by the New Ondřejov Solar Radio Spectrograph. *Solar Phys.* **253**, 95. DOI. ADS.
- Jiříčka, K., Karlický, M., Kepka, O., Tlamicha, A.: 1993, Fast drift burst observations with the new Ondřejov radiospectrograph. *Solar Phys.* **147**, 203. DOI. ADS.
- Karlický, M.: 1988, Response of the current sheet to a time-limited enhancement of electrical resistivity. *Bulletin of the Astronomical Institutes of Czechoslovakia* **39**, 13. ADS.
- Karlický, M.: 2004, Series of high-frequency slowly drifting structures mapping the flare magnetic field reconnection. *Astron. Astrophys.* **417**, 325. DOI. ADS.
- Karlický, M.: 2008, Separation of Accelerated Electrons and Positrons in the Relativistic Reconnection. *Astrophys. J.* **674**, 1211. DOI. ADS.
- Karlický, M.: 2013, Radio continua modulated by waves: Zebra patterns in solar and pulsar radio spectra? *Astron. Astrophys.* **552**, A90. DOI. ADS.
- Karlický, M., Bárta, M.: 2007, Drifting pulsating structures generated during tearing and coalescence processes in a flare current sheet. *Astron. Astrophys.* **464**, 735. DOI. ADS.
- Karlický, M., Bárta, M.: 2011, Successive Merging of Plasmoids and Fragmentation in a Flare Current Sheet and Their X-Ray and Radio Signatures. *Astrophys. J.* **733**, 107. DOI. ADS.
- Karlický, M., Rybák, J.: 2017, Oscillation Maps in the Broadband Radio Spectrum of the 1 August 2010 Event. *Solar Phys.* **292**, 1. DOI. ADS.
- Karlický, M., Bárta, M., Rybák, J.: 2010, Radio spectra generated during coalescence processes of plasmoids in a flare current sheet. *Astron. Astrophys.* **514**, A28. DOI. ADS.
- Karlický, M., Mészárosóvá, H., Jelínek, P.: 2013, Radio fiber bursts and fast magnetoacoustic wave trains. *Astron. Astrophys.* **550**, A1. DOI. ADS.
- Karlický, M., Zlobec, P., Mészárosóvá, H.: 2010, Subsecond (0.1 s) Pulsations in the 11 April 2001 Radio Event. *Solar Phys.* **261**, 281. DOI. ADS.
- Kliem, B., Karlický, M., Benz, A.O.: 2000, Solar flare radio pulsations as a signature of dynamic magnetic reconnection. *Astron. Astrophys.* **360**, 715. ADS.
- Konkol, P., Murawski, K., Lee, D., Weide, K.: 2010, Numerical simulations of the attenuation of the fundamental slow magnetoacoustic standing mode in a gravitationally stratified solar coronal arcade. *Astron. Astrophys.* **521**, A34. DOI. ADS.
- Kumar, P., Cho, K.-S.: 2013, Simultaneous EUV and radio observations of bidirectional plasmoids ejection during magnetic reconnection. *Astron. Astrophys.* **557**, A115. DOI. ADS.
- Kumar, P., Nakariakov, V.M., Cho, K.-S.: 2016, Observation of a Quasiperiodic Pulsation in Hard X-Ray, Radio, and Extreme-ultraviolet Wavelengths. *Astrophys. J.* **822**, 7. DOI. ADS.
- Kundu, M.R.: 1965, *Solar radio astronomy*, Interscience, New York, p. 27. ADS.
- Kupriyanova, E.G., Melnikov, V.F., Nakariakov, V.M., Shibasaki, K.: 2010, Types of Microwave Quasi-Periodic Pulsations in Single Flaring Loops. *Solar Phys.* **267**, 329. DOI. ADS.

- Kuznetsov, A.A.: 2006, Generation of Intermediate Drift Bursts by Magnetohydrodynamic Waves in the Solar Corona. *Solar Phys.* **237**, 153. DOI. ADS.
- Mann, G., Karlický, M., Motschmann, U.: 1987, On the intermediate drift burst model. *Solar Phys.* **110**, 381. DOI. ADS.
- Meegan, C., Lichti, G., Bhat, P.N., Bissaldi, E., Briggs, M.S., Connaughton, V., Diehl, R., Fishman, G., Greiner, J., Hoover, A.S., van der Horst, A.J., von Kienlin, A., Kippen, R.M., Kouveliotou, C., McBreen, S., Paciesas, W.S., Preece, R., Steinle, H., Wallace, M.S., Wilson, R.B., Wilson-Hodge, C.: 2009, The Fermi Gamma-ray Burst Monitor. *Astrophys. J.* **702**, 791. DOI. ADS.
- Mészárosová, H., Rybák, J., Karlický, M.: 2011, Separation of drifting pulsating structures in a complex radio spectrum of the 2001 April 11 event. *Astron. Astrophys.* **525**, A88. DOI. ADS.
- Mészárosová, H., Karlický, M., Rybák, J., Fárnik, F., Jiříčka, K.: 2006, Long period variations of dm-radio and X-ray fluxes in three X-class flares. *Astron. Astrophys.* **460**, 865. DOI. ADS.
- Mészárosová, H., Karlický, M., Jelínek, P., Rybák, J.: 2014, Magnetoacoustic Waves Propagating along a Dense Slab and Harris Current Sheet and their Wavelet Spectra. *Astrophys. J.* **788**, 44. DOI. ADS.
- Nakariakov, V.M., Melnikov, V.F.: 2009, Quasi-Periodic Pulsations in Solar Flares. *Space Sci. Rev.* **149**, 119. DOI. ADS.
- Nakariakov, V.M., Pascoe, D.J., Arber, T.D.: 2005, Short Quasi-Periodic MHD Waves in Coronal Structures. *Space Sci. Rev.* **121**, 115. DOI. ADS.
- Nakariakov, V.M., Tsiklauri, D., Kelly, A., Arber, T.D., Aschwanden, M.J.: 2004, Acoustic oscillations in solar and stellar flaring loops. *Astron. Astrophys.* **414**, L25. DOI. ADS.
- Nakariakov, V.M., Foullon, C., Verwichte, E., Young, N.P.: 2006, Quasi-periodic modulation of solar and stellar flaring emission by magnetohydrodynamic oscillations in a nearby loop. *Astron. Astrophys.* **452**, 343. DOI. ADS.
- Nakariakov, V.M., Inglis, A.R., Zimovets, I.V., Foullon, C., Verwichte, E., Sych, R., Myagkova, I.N.: 2010, Oscillatory processes in solar flares. *Plasma Physics and Controlled Fusion* **52**(12), 124009. DOI. ADS.
- Nakariakov, V.M., Pilipenko, V., Heilig, B., Jelínek, P., Karlický, M., Klimushkin, D.Y., Kolotkov, D.Y., Lee, D.-H., Nisticò, G., Van Doorselaere, T., Verth, G., Zimovets, I.V.: 2016, Magnetohydrodynamic Oscillations in the Solar Corona and Earth's Magnetosphere: Towards Consolidated Understanding. *Space Sci. Rev.* **200**, 75. DOI. ADS.
- Nishizuka, N., Karlický, M., Janvier, M., Bárta, M.: 2015, Particle Acceleration in Plasmoid Ejections Derived from Radio Drifting Pulsating Structures. *Astrophys. J.* **799**, 126. DOI. ADS.
- Nisticò, G., Pascoe, D.J., Nakariakov, V.M.: 2014, Observation of a high-quality quasi-periodic rapidly propagating wave train using SDO/AIA. *Astron. Astrophys.* **569**, A12. DOI. ADS.
- Norman, C.A., Smith, R.A.: 1978, Kinetic processes in solar flares. *Astron. Astrophys.* **68**, 145. ADS.
- Ofman, L., Wang, T.: 2002, Hot Coronal Loop Oscillations Observed by SUMER: Slow Magnetosonic Wave Damping by Thermal Conduction. *Astrophys. J. Lett.* **580**, L85. DOI. ADS.
- Ofman, L., Wang, T.J., Davila, J.M.: 2012, Slow Magnetosonic Waves and Fast Flows in Active Region Loops. *Astrophys. J.* **754**, 111. DOI. ADS.
- Ohyama, M., Shibata, K.: 1998, X-Ray Plasma Ejection Associated with an Impulsive Flare on 1992 October 5: Physical Conditions of X-Ray Plasma Ejection. *Astrophys. J.* **499**, 934. DOI. ADS.
- Pascoe, D.J., De Moortel, I.: 2014, Standing Kink Modes in Three-dimensional Coronal Loops. *Astrophys. J.* **784**, 101. DOI. ADS.
- Pohjolainen, S., van Driel-Gesztelyi, L., Culhane, J.L., Manoharan, P.K., Elliott, H.A.: 2007, CME Propagation Characteristics from Radio Observations. *Solar Phys.* **244**, 167. DOI. ADS.
- Roberts, B., Edwin, P.M., Benz, A.O.: 1984, On coronal oscillations. *Astrophys. J.* **279**, 857. DOI. ADS.
- Selwa, M., Murawski, K., Solanki, S.K.: 2005, Excitation and damping of slow magnetosonic standing waves in a solar coronal loop. *Astron. Astrophys.* **436**, 701. DOI. ADS.
- Tan, B.: 2008, Observable Parameters of Solar Microwave Pulsating Structure and Their Implications for Solar Flare. *Solar Phys.* **253**, 117. DOI. ADS.

- Torrence, C., Compo, G.P.: 1998, A Practical Guide to Wavelet Analysis. *Bulletin of the American Meteorological Society* **79**, 61. DOI. ADS.
- Treumann, R.A., Guedel, M., Benz, A.O.: 1990, Alfven wave solitons and solar intermediate drift bursts. *Astron. Astrophys.* **236**, 242. ADS.
- Van Doorselaere, T., Kupriyanova, E.G., Yuan, D.: 2016, Quasi-periodic Pulsations in Solar and Stellar Flares: An Overview of Recent Results (Invited Review). *Solar Phys.* **291**, 3143. DOI. ADS.
- Wang, T.J., Solanki, S.K., Innes, D.E., Curdt, W.: 2005, Initiation of hot coronal loop oscillations: Spectral features. *Astron. Astrophys.* **435**, 753. DOI. ADS.
- Watanabe, K., Masuda, S., Segawa, T.: 2012, Hinode Flare Catalogue. *Solar Phys.* **279**, 317. DOI. ADS.